Neuron
Article

Synaptic Mechanisms Underlying Sparse Coding of Active Touch

Sylvain Crochet,[1,2] James F.A. Poulet,[1,3,4] Yves Kremer,[1] and Carl C.H. Petersen[1,*]
[1]Laboratory of Sensory Processing, Brain Mind Institute, Faculty of Life Sciences, École Polytechnique Fédérale de Lausanne (EPFL), CH-1015 Lausanne, Switzerland
[2]INSERM U1028/CNRS UMR5292 Integrative Physiology of Brain Arousal Systems, Lyon Neuroscience Research Center, 69500 Bron, France
[3]Department of Neuroscience, Max-Delbrück Center for Molecular Medicine, Berlin-Buch, 10392 Berlin, Germany
[4]Neurocure Neuroscience Research Center, Charité-Universitätsmedizin Berlin, 10117 Berlin, Germany
*Correspondence: carl.petersen@epfl.ch
DOI 10.1016/j.neuron.2011.02.022

SUMMARY

Sensory information is actively gathered by animals, but the synaptic mechanisms driving neuronal circuit function during active sensory processing are poorly understood. Here, we investigated the synaptically driven membrane potential dynamics during active whisker sensation using whole-cell recordings from layer 2/3 pyramidal neurons in the primary somatosensory barrel cortex of behaving mice. Although whisker contact with an object evoked rapid depolarization in all neurons, these touch responses only drove action potentials in ~10% of the cells. Such sparse coding was ensured by cell-specific reversal potentials of the touch-evoked response that were hyperpolarized relative to action potential threshold for most neurons. Intercontact interval profoundly influenced touch-evoked postsynaptic potentials, interestingly without affecting the peak membrane potential of the touch response. Dual whole-cell recordings indicated highly correlated membrane potential dynamics during active touch. Sparse action potential firing within synchronized cortical layer 2/3 microcircuits therefore appears to robustly signal each active touch response.

INTRODUCTION

Animals actively gather sensory information through self-generated movements. For example, eye movements are used to foveate interesting regions of visual space. Self-generated eye movements, therefore, in part determine the visual sensory input that falls upon the retina. Active sensing is also obvious for somatosensation, where finger movements are used to explore object shape and texture. Through internally generated movements, animals thus determine a large part of the sensory information that they receive. In order to understand perception it is therefore important to study how sensory information is actively acquired.

The rodent whisker sensorimotor system is an attractive and relatively simple model system for studying mammalian active sensory processing (reviewed in Brecht, 2007; Petersen, 2007; Diamond et al., 2008). During exploratory behavior, rodents move their whiskers back and forth at high frequencies (typically 5–20 Hz) scanning their surroundings to obtain tactile information about nearby objects. Rodents can use their whiskers to actively gather spatial (Hutson and Masterton, 1986; Harris et al., 1999; Krupa et al., 2004; Knutsen et al., 2006; Curtis and Kleinfeld, 2009; O'Connor et al., 2010) and textural tactile sensory information (Guić-Robles et al., 1989; Carvell and Simons, 1990; von Heimendahl et al., 2007; Jadhav et al., 2009).

Extracellular recordings in the barrel cortex of awake behaving rodents have begun to shed light on the action potential coding of tactile sensory information (Krupa et al., 2004; von Heimendahl et al., 2007; Stüttgen and Schwarz, 2008; Jadhav et al., 2009; Curtis and Kleinfeld, 2009; Gerdjikov et al., 2010; O'Connor et al., 2010). However, little is known about the mechanisms driving the spike coding of whisker sensory perception. Action potentials are driven by synaptic interactions, with the majority of cortical unitary postsynaptic potentials being small in amplitude evoking only subthreshold changes in membrane potential (Vm) (Crochet et al., 2005; Bruno and Sakmann, 2006; Lefort et al., 2009). Previous studies have investigated subthreshold Vm dynamics evoked by passive whisker stimuli in anesthetised animals (Moore and Nelson, 1998; Zhu and Connors, 1999; Petersen et al., 2003; Brecht et al., 2003; Wilent and Contreras, 2005; Katz et al., 2006; Higley and Contreras, 2006; Heiss et al., 2008). However, there are important changes in cortical dynamics during active sensory exploration compared to quiet wakefulness or anesthesia. Quiet wakefulness is characterized in layer 2/3 neurons of mouse barrel cortex by large-amplitude, slow (1–5 Hz), and highly synchronized Vm fluctuations; a low firing rate of pyramidal cells and non-fast-spiking GABAergic neurons; but a high firing rate of fast-spiking GABAergic neurons (Crochet and Petersen, 2006; Poulet and Petersen, 2008; Gentet et al., 2010). During active whisking in air, the slow activity is suppressed and barrel cortex neurons exhibit fast low-amplitude Vm fluctuations that are less correlated in nearby neurons and the input resistance of pyramidal cells is slightly reduced (Crochet and Petersen, 2006; Poulet and Petersen, 2008; Gentet et al., 2010). The firing rate of pyramidal cells on average does not change significantly between quiet and whisking states; but the activity of GABAergic neurons is reorganized such that non-fast-spiking GABAergic neurons increase firing rates during

whisking, whereas fast-spiking GABAergic neurons decrease firing rates, resulting in similar firing rates of both classes of GABAergic neurons during whisking (Crochet and Petersen, 2006; Poulet and Petersen, 2008; Gentet et al., 2010). These profound changes in cortical network dynamics also correlate with dramatic changes in sensory processing (Fanselow and Nicolelis, 1999; Castro-Alamancos, 2004; Hentschke et al., 2006; Crochet and Petersen, 2006; Ferezou et al., 2007). It is therefore of crucial importance to study Vm dynamics in awake animals actively sensing and exposed to natural stimuli.

Here, through whole-cell Vm recordings of layer 2/3 pyramidal neurons in the mouse barrel cortex, we investigate how tactile information from a single whisker (C2) is processed during active touch. Sensory information relating to the C2 whisker is signaled to the C2 barrel column of primary somatosensory cortex, an anatomically defined region of the mouse brain with a diameter of approximately 250 μm containing around 6500 neurons (Lefort et al., 2009). Investigations of this specific cortical column have begun to yield quantitative information relating to its synaptic structure (Knott et al., 2002), synaptic connectivity (Lefort et al., 2009), and functional operation during behavior (Crochet and Petersen, 2006; Poulet and Petersen, 2008; Gentet et al., 2010). The convergence of techniques focusing upon a single well-defined cortical column may help toward a quantitative and mechanistic understanding of how a specific neocortical microcircuit processes sensory information.

RESULTS

Whole-Cell Membrane Potential Recordings during Active Touch

Whole-cell recordings were obtained from head-restrained mice and the Vm dynamics of layer 2/3 neurons located in the C2 barrel column were correlated with C2 whisker-related behavior through high-speed filming (500 Hz) under infrared illumination (Figures 1A and 1B). Objects could be inserted on the millisecond timescale into the trajectory of the C2 whisker in one of two different locations using piezoactuators (schematically indicated as red and blue objects in Figure 1A). The C2 whisker-related behavior was quantified off-line based on the high-speed filming (Figure 1C; Movies S1 and S2 available online). We distinguished between three different behavioral periods (Figures 1B and 1C): free whisking (W, when both piezoactuators were raised up and the whisker moved back and forth freely without touching any object); active touch (T, when one of the piezoactuators was lowered and the mouse actively moved the C2 whisker repetitively against the object causing a bending of the whisker); and quiet wakefulness (Q, when the awake mouse was not moving its whisker). The recorded neurons were labeled with biocytin for post-hoc anatomical identification and location relative to the barrel map (Figure 1D). Membrane potential dynamics evoked by C2 whisker touch (Figure 1E) were compared with periods of free whisking and quiet waking.

Whisker Behavior Modulates Layer 2/3 Cortical Dynamics

We analyzed data from 18 whole-cell recordings of layer 2/3 cells in the C2 barrel column (each cell was recorded in a different mouse), of which 14 were sufficiently well-stained to be anatomically identified and found to be pyramidal neurons (Table S1). On average the Vm was most hyperpolarized during quiet waking (Q; mean ± standard deviation [SD] −60.5 ± 7.5 mV; median −60.7 mV; range −73.8 to −44.7 mV), depolarized during free whisking (W; mean ± SD −58.4 ± 8.3 mV; median −57.7 mV; range −73.7 to −36.9 mV), and was significantly more depolarized during active touch (T; mean ± SD −55.4 ± 7.7 mV; median −57.2 mV; range −70.6 to −37.0 mV) (Figure 2A and Table S2). Compared to free whisking, during an active touch sequence the Vm of layer 2/3 neurons on average depolarized by 3.0 ± 2.9 mV (median 3.0 mV; range −2.2 to +6.9 mV). Vm variance was significantly lower during free whisking than during quiet wakefulness or active touch (Figure 2B). The low Vm variance during free whisking (when there is no incoming touch information) may help provide a reduced noise background enhancing the detection of sensory-evoked signals during active touch.

The mean action potential firing rates (Figure 2C and Table S2) indicate that spike rates increased during active touch (1.7 ± 5.0 Hz; median 0.2 Hz; range 0.0 to 20.8 Hz) as compared to quiet wakefulness (0.2 ± 0.2 Hz; median 0.1 Hz; range 0.0 to 0.5 Hz) and free whisking (0.3 ± 0.9 Hz; median 0.04 Hz; range 0.0 to 3.9 Hz). For most neurons the firing rate of layer 2/3 pyramidal cells remained low in all conditions, in good agreement with recent awake extracellular recordings of identified layer 2/3 pyramidal cells (de Kock and Sakmann, 2009; Sakata and Harris, 2009) and awake two-photon calcium imaging in layer 2/3 (Greenberg et al., 2008; O'Connor et al., 2010).

Low-frequency Vm dynamics dominated the Fast Fourier Transform (FFT) during all behavioral periods, with a near linear decrease at higher frequencies when plotted on log-log scale axes (Figure 2D) similar to observations from EEG recordings (Buzsáki and Draguhn, 2004). Slow Vm fluctuations (1–5 Hz) were significantly more prominent during quiet wakefulness than during free whisking (Crochet and Petersen, 2006; Poulet and Petersen, 2008; Gentet et al., 2010) or active touch (Figures 2D and 2E). High-frequency Vm changes (30 to 100 Hz) were significantly increased during active touch compared to quiet wakefulness or free whisking (Figures 2D and 2E). These higher-frequency Vm dynamics are likely to be driven by the rapid and large-amplitude depolarizations evoked by individual touch responses.

Fast Membrane Potential Dynamics during Whisking and Active Touch

Analysis on the millisecond timescale revealed further important correlations between the C2 whisker-related behavior and neuronal Vm. We averaged the Vm across many individual whisking cycles aligned to the peak of protraction during free whisking and found small-amplitude phase-locked Vm fluctuations, which weakly influenced action potential firing (Figure 3A and Figure S1) (Fee et al., 1997; Crochet and Petersen, 2006; Poulet and Petersen, 2008; Curtis and Kleinfeld, 2009; de Kock and Sakmann, 2009). Averaging traces aligned to the onset of whisker-object contact revealed a rapid and large-amplitude depolarizing touch response in many neurons, which was accompanied in some neurons by a transient elevation of action

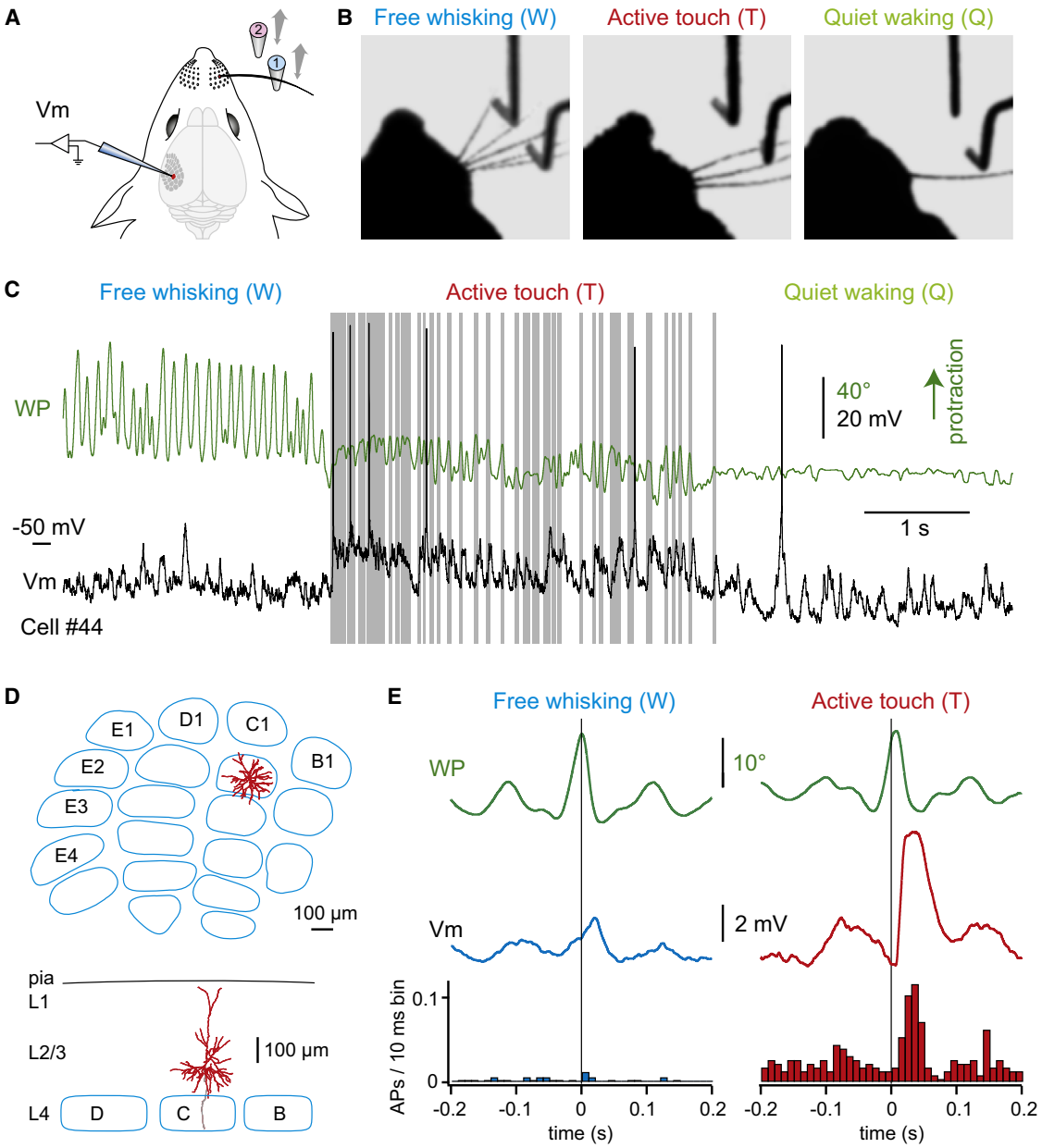

Figure 1. Whole-Cell Recording during Quiet Waking, Free Whisking, and Active Touch

(A) Schematic drawing of whole-cell recording of membrane potential (Vm) from the barrel cortex. Objects could be rapidly inserted into the whisker path at either a caudal (blue, position 1) or a rostral (red, position 2) location.

(B) Overlay of images from high-speed filming of free whisking (W), active touch with the caudal object (T), and quiet waking (Q).

(C) Whole-cell Vm recording (black trace) from a layer 3 pyramidal neuron within the C2 barrel column (cell #44) with overlaid whisker position (WP, green trace, protraction upward) and whisker-object contacts (gray bars) quantified from the high-speed filming. The mouse is freely whisking then repetitively touches the object and enters a period of quiet waking.

(D) Reconstructed dendrites (red) and descending primary axon (gray) within the barrel map (blue) from the recording shown in (B) and (C); tangential (top) and normal (bottom) views are shown.

(E) For the same recording, the average WP (green), Vm, and peristimulus time histograms of action potential firing (PSTH) were computed by aligning to the peak of the protraction for free whisking episodes (left, blue) or the onset of whisker-object contact during active touch (right, red).

potential firing (Figure 3B). We found that all C2 column layer 2/3 neurons responded significantly to C2 whisker-object contact by a transient depolarization, whereas only 11/17 neurons showed significant free whisking Vm modulation (Table S2). The touch-evoked postsynaptic potential (PSP) response was much larger than the free whisking Vm modulation for every recorded neuron

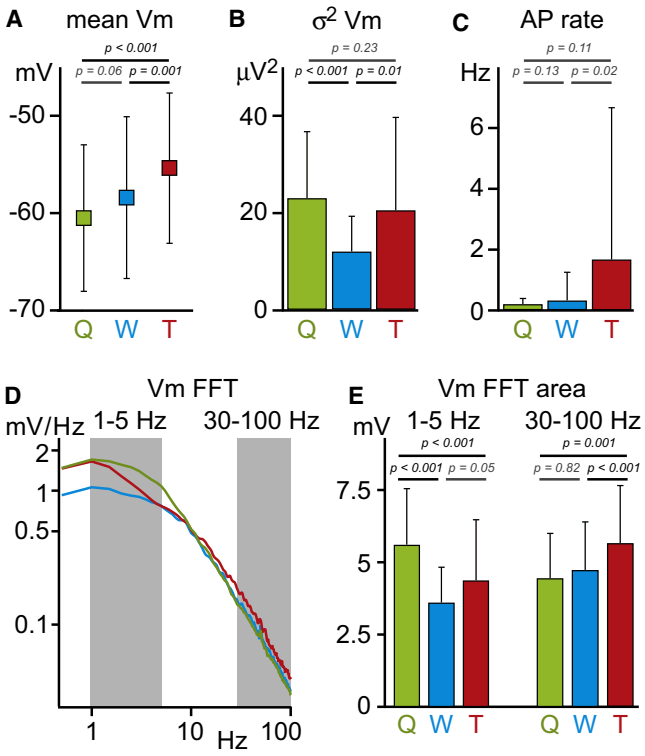

Figure 2. State-Dependent Membrane Potential Dynamics during Quiet Waking, Free Whisking, and Active Touch

(A) The mean membrane potential (Vm) was quantified across 18 neurons located in layer 2/3 of the C2 barrel column during quiet waking (Q, green), free whisking (W, blue), and active touch (T, red).

(B) Vm variance (σ^2).

(C) Action potential firing rates.

(D) Population average of the Fast Fourier Transform (FFT) of the Vm plotted on log-log scale for quiet waking (green), free whisking (blue), and active touch (red).

(E) FFT area for low (1–5 Hz) and high (30–100 Hz) frequency Vm fluctuations. Data are presented as mean ± SD. Significance after Bonferonni correction ($p < 0.016$) was assessed using the Wilcoxon Signed Rank test; p values are in black (significant) and gray (nonsignificant).

in layer 2/3 (touch to whisk ratio: mean 73 ± 253; median 10.6; range 3.6 to 1056.0); and, similarly, the change in spike rates evoked by active contacts was much larger than the free whisking spike rate modulation (Figure 3C).

Although all layer 2/3 neurons responded with a significant depolarizing touch-evoked PSP, action potential firing in response to whisker-object contact occurred only in a small subset of the neurons. The mean probability that a layer 2/3 neuron in the C2 barrel column fires at least one action potential within the next 50 ms following a contact of the C2 whisker with an object was 0.10 ± 0.21 (median 0.03; range 0.00 to 0.88) (Figure 4A and Table S2). Thus about 10% of the layer 2/3 pyramidal neurons in the aligned cortical column fire in response to each principal whisker-object contact. Only one neuron in our data set fired reliably, and it appears that a very small number of neurons contribute to most of the evoked spiking activity (only 4/18 cells discharged with a probability above 10% per contact, whereas 5/18 cells never fired in response to active touch). Neurons located in deeper layer 2/3 fired significantly more touch-evoked action potentials at significantly shorter latencies (Figure 4A).

Whole-cell recordings could alter the firing probability of the recorded neurons. In order to examine this possibility, we performed an independent set of experiments recording action potential activity extracellularly. To specifically record from excitatory neurons, we targeted the recording electrode to GFP-negative neurons (n = 16 neurons in 8 mice) visualized through two-photon microscopy in the GAD67-GFP knockin mouse, in which all layer 2/3 GABAergic neurons express GFP (Tamamaki et al., 2003; Gentet et al., 2010). Touch-evoked action potential firing in these juxtacellular recordings of layer 2/3 excitatory neurons was sparse. The mean probability of firing an action potential within 50 ms of a contact was 0.12 ± 0.23 (median 0.02; range 0.00 to 0.87). Only 4/16 excitatory neurons fired with a probability of above 10% per contact, whereas 5/16 excitatory neurons never fired in response to active touch. The distribution of spiking probability across the population of excitatory neurons was therefore very similar in juxtacellular recordings to that found with whole-cell recordings (Figure 4A, compare intra with juxta).

Although significant in all C2 column neurons, the PSP response to active touch varied strongly from cell to cell in amplitude (mean 6.3 ± 3.0 mV; median 6.7 mV; range 0.5 to 11.0 mV); latency (mean 8.6 ± 2.7 ms; median 8.7 ms; range 5.3 to 12.7 ms); time-to-peak (mean 16.0 ± 9.9 ms; median 13.8 ms; range 4.9 to 37.2 ms); duration (mean 52.5 ± 27.0 ms; median 51.8 ms; range 9.1 to 103.1 ms); and rate of rise (slope, mean 0.56 ± 0.49 V/s; median 0.41 V/s; range 0.09 to 1.52 V/s) (Figures 4B). Cells with shorter latency tended to exhibit larger-amplitude subthreshold responses and neurons exhibiting a fast time-to-peak also tended to have a shorter-duration response (data not shown). Neurons recorded deeper in L2/3 responded with PSPs of larger-amplitude depolarizations, shorter latencies, shorter-duration responses, and faster rates of rise (PSP slope) (Figure 4B). Therefore, deeper neurons, located in layer 3, preferentially signal each individual contact with high temporal precision, whereas the more superficial layer 2 neurons preferentially integrate touch responses over a longer timescale.

Nine identified layer 2/3 pyramidal neurons were recorded in adjacent barrel columns (Table S1). The grand averaged response to active touch of the C2 whisker with an object reveals a smaller amplitude response with longer latency in the surrounding cortical columns, but otherwise sharing a similar range of response properties (Figure S2). That the touch response spreads to neighboring columns is consistent with voltage-sensitive dye imaging data showing that a large area of cortex can depolarize in response to single whisker active touch in awake mice (Ferezou et al., 2007). These data are also consistent with the broad subthreshold receptive fields of layer 2/3 neurons evoked by passive whisker deflection recorded under anesthesia (Moore and Nelson, 1998; Zhu and Connors, 1999; Brecht et al., 2003).

Hyperpolarized Reversal Potentials for Touch Responses

Consecutive touches evoked different amplitude touch PSP responses (Figure 5A) (coefficient of variation mean ± SD

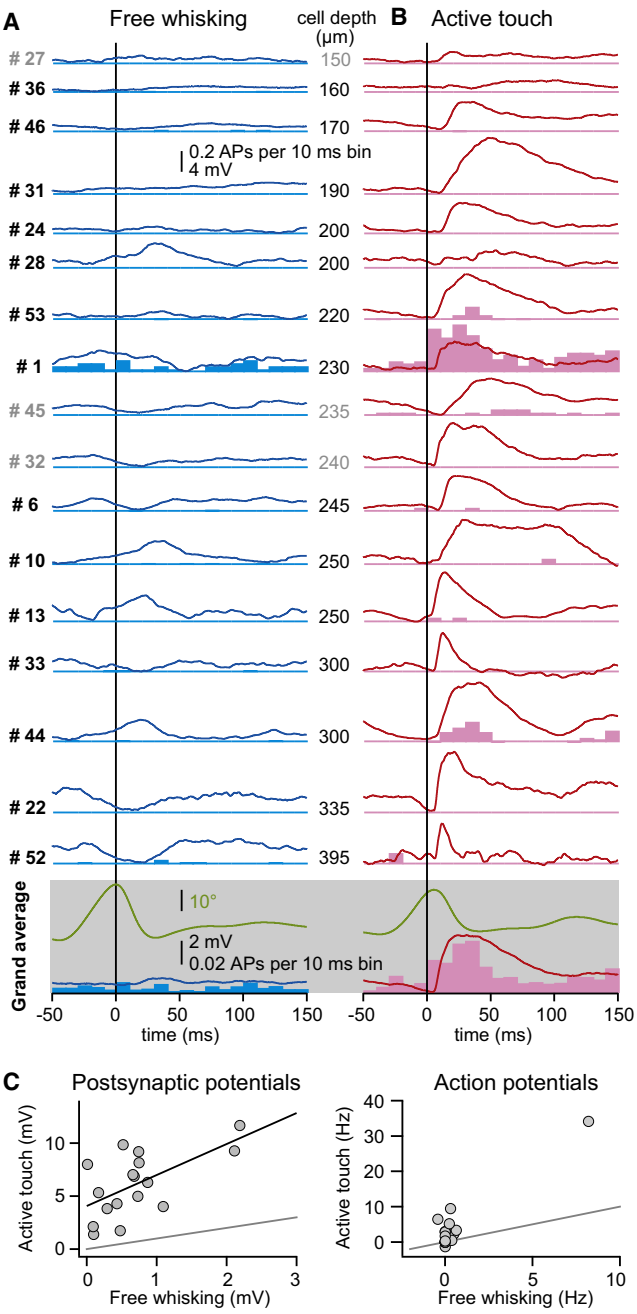

Figure 3. Fast Membrane Potential Dynamics during Free Whisking and Active Touch

(A) Protraction triggered Vm averages and peristimulus time histograms (PSTH) during free whisking (blue) computed from whisker movements with protraction amplitude ranging from 25° to 35°. The bottom panel shows the population average of the whisker positions (WP, green), Vm, and PSTH. Cell numbers are indicated on the left side (black labels indicate identified pyramidal neurons). Cell depth is indicated in between (A) and (B); cells are ordered from superficial (top) to deep (bottom).

(B) Whisker-object contact triggered Vm averages and PSTH during active touch (red) for each recorded neuron (as for A) computed for contacts with preceding intercontact interval > 80 ms. The bottom panels show the population average of the whisker positions (WP, green), Vm, and PSTH.

(C) Cell-by-cell comparison between the active touch response and free whisking modulation. Whisker movements and contacts with similar protraction amplitude (25° to 35°) were selected to compare free whisking Vm modulation and touch responses. The free whisking Vm modulation was measured at the same time intervals as the amplitude of the postsynaptic potential evoked by active touch for each cell (left; black line, linear regression with $r = 0.60$ and $p < 0.01$; gray line, unitary slope). The difference of the mean firing rate was measured for 10 ms time windows at the minimum and at the peak of the subthreshold average Vm for active touch and for free whisking (right; gray line, unitary slope).

1.4 ± 0.7; median 1.0; range 0.4 to 3.1). Part of the variability of the touch response could be accounted for by considering the neuronal membrane potential immediately preceding the response onset, which profoundly influenced the PSP amplitude. Touch responses evoked at spontaneously hyperpolarized precontact Vm were larger in amplitude compared to touch responses occurring during spontaneously depolarized membrane potentials (Figure 5B). Indeed, at the most depolarized precontact membrane potentials, the touch response was hyperpolarizing (Figure 5B). Plotting the active touch response amplitude as a function of the precontact Vm revealed a close to linear relationship (Figure 5C). The correlation between response amplitude and precontact Vm was significant (α = 0.05) in all 17 neurons tested (cell #36 had a complex depolarizing-hyperpolarizing response and was not included in the subsequent active touch response dynamic analysis; see Table S1). The mean coefficient of correlation was −0.62 ± 0.11 (median −0.60; range −0.41 to −0.86), indicating that precontact Vm accounted for 40% ± 15% (median 36%; range 17% to 74%) of the variability of the response amplitude. From such linear regressions for each recorded neuron, we determined the reversal potential of the touch response (above which the touch response became hyperpolarizing) with respect to spontaneous precontact Vm. The reversal potentials for the touch response in 16/17 neurons were hyperpolarized (mean −46.9 ± 9.3 mV; median −45.3 mV; range −68.9 to −28.5 mV) relative to action potential threshold (mean −38.7 ± 2.9 mV; median −39.2 mV; range −43.9 to −33.5 mV) (Figures 5D and 5E). There was a strong correlation between the touch response reversal potential computed at the peak of the PSP and the probability of touch-evoked action potential firing (Figure 5F). Computing the reversal potential of the PSP at different time points yielded similar correlations (Figures S3A and S3B), indicating that the reversal potential has a robust effect on action potential probability independent of the exact time-point of quantification. The only neuron (Cell #1) that fired reliably (AP probability of 0.88 per contact) was also the only neuron with a touch response reversal potential (−28.5 mV) that was more depolarized than its action potential threshold (−33.7 mV). In contrast, we did not find any significant correlations between AP probability and PSP amplitude, PSP rise time or PSP slope (Figure S3C). The reversal potential of the touch response therefore appears to be a key determinant of the spike output of layer 2/3 pyramidal neurons during active sensory perception.

These hyperpolarized reversal potentials suggest a prominent and rapid inhibitory GABAergic contribution to the active touch responses (Figure S3A), similar to the response evoked by

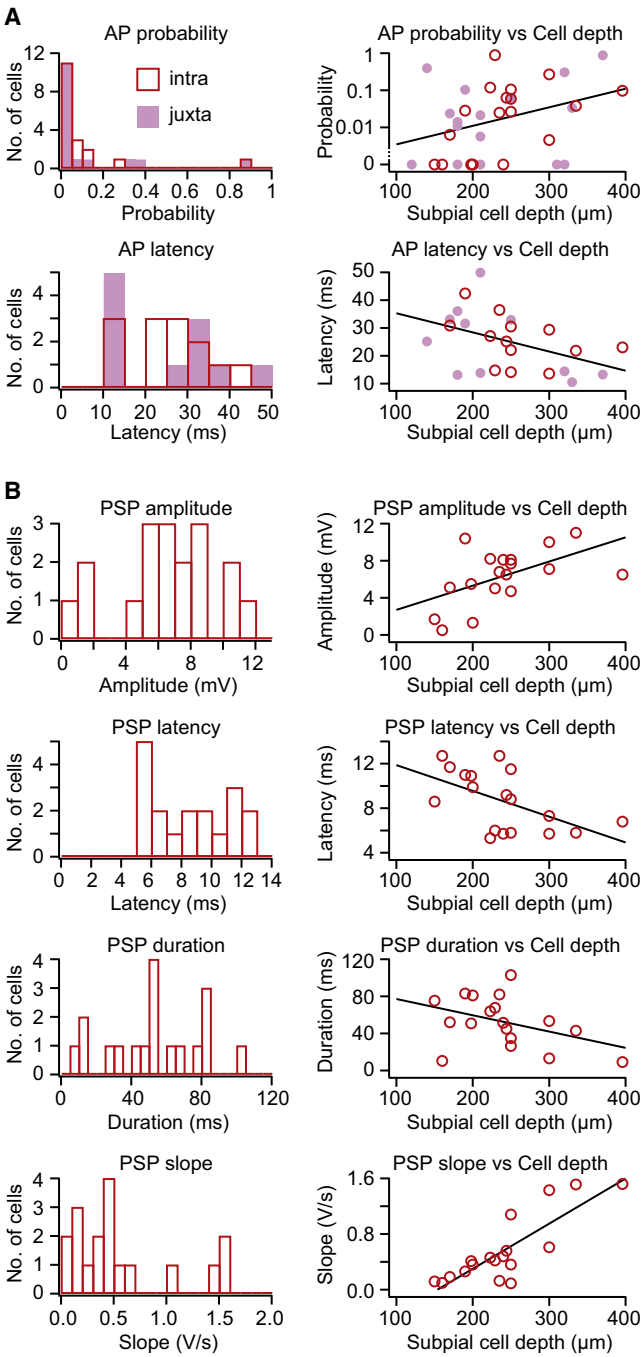

Figure 4. Properties of the Active Touch Response

(A) Distribution of action potential firing probability (upper left) computed for a 50 ms time window following contact onset and distribution of first spike latency from contact onset (lower left). Red open histogram bins show data from whole-cell membrane potential recordings (labeled intra). Purple shaded bins show data from juxtacellular recordings (labeled juxta). The relationship of firing probability (upper right) and first spike latency (lower right) are plotted as a function of somatic subpial depth. Touch-evoked AP firing increases significantly with depth (log AP probability versus cell depth: $r = 0.36$; $p < 0.05$) and AP latency decreases significantly with depth ($r = -0.44$; $p < 0.05$).

(B) Distributions of the mean amplitude, latency, half-amplitude duration, and rate of rise (slope) of the subthreshold postsynaptic potential (PSP) active touch response (left). The touch PSPs in neurons located deeper in layer 2/3 had larger amplitude ($r = 0.55$, $p < 0.05$), shorter latency ($r = -0.55$; $p < 0.05$), shorter duration ($r = -0.41$; $p < 0.05$), and faster rate of rise (slope) ($r = 0.83$; $p < 0.001$) (right).

passive whisker deflection under anesthesia (Petersen et al., 2003; Wilent and Contreras, 2005; Okun and Lampl, 2008). A necessary condition for a contribution of inhibition to the active touch response is for GABAergic neurons to fire action potentials in response to active touch. We therefore targeted extracellular recordings to GFP-labeled GABAergic neurons (n = 15) in GAD67-GFP mice (Tamamaki et al., 2003; Liu et al., 2009; Gentet et al., 2010) (Figure 5G). During active touch sequences, GABAergic neurons on average fired at higher rates compared to excitatory pyramidal neurons (excitatory whole-cell 1.7 ± 5.0 Hz; excitatory juxtacellular 2.1 ± 4.3 Hz; GABAergic juxtacellular 10.6 ± 20.5 Hz), with a clear short-latency modulation of spike rate evoked by each touch (Figure 5H). GABAergic neurons fired with higher probability (mean 0.27 ± 0.38; median 0.09; range 0 to 1) during the 50 ms following whisker-object contact, as compared to excitatory neurons (combined whole-cell and excitatory juxtacellular data, mean 0.11 ± 0.22; median 0.02; range 0 to 0.88; n = 34) (Figure 5I). For these juxtacellular recordings from GABAergic neurons, we found that 7/15 inhibitory neurons fired with a probability of above 10% per contact; whereas 3/15 inhibitory neurons never fired in response to active touch. These data are consistent with an important and rapid recruitment of inhibition during active touch, which is likely to impose the hyperpolarized reversal potentials for the touch-evoked PSPs found in excitatory layer 2/3 neurons.

Intercontact Interval Strongly Affects the Touch Response

Internal cortical dynamics and precontact membrane potential therefore play a major role in governing the trial-by-trial touch-evoked PSP, but one would also expect important contributions to the response variability mediated by differences in kinetics during different whisker-object contacts. However, in agreement with previous local field potential measurements (Hentschke et al., 2006), in most neurons we found that the amplitude of the touch-evoked PSP was modulated neither by precontact velocity nor contact duration (Table S2). However, we did find a strong influence of the intercontact interval (ICI) upon the touch response.

The first whisker-object contact in a touch sequence generally evoked the largest membrane potential depolarization (Figures 6A and 6E). Subsequent touches on average evoked smaller depolarizations, indicating a dependence upon the recent history of C2 whisker-related touches (Figure 6I). Averaging active touch responses for different intercontact interval ranges revealed a decrease in response amplitude as the ICI becomes smaller (Figures 6B and 6F). In order to evaluate further the impact of ICI, we plotted the amplitude of the touch response as a function of the preceding intercontact interval (Figures 6C and 6G). Spearman's rank test revealed a significant modulation of response amplitude by ICI in 13/17 neurons. For those neurons, the time course of the recovery of the touch

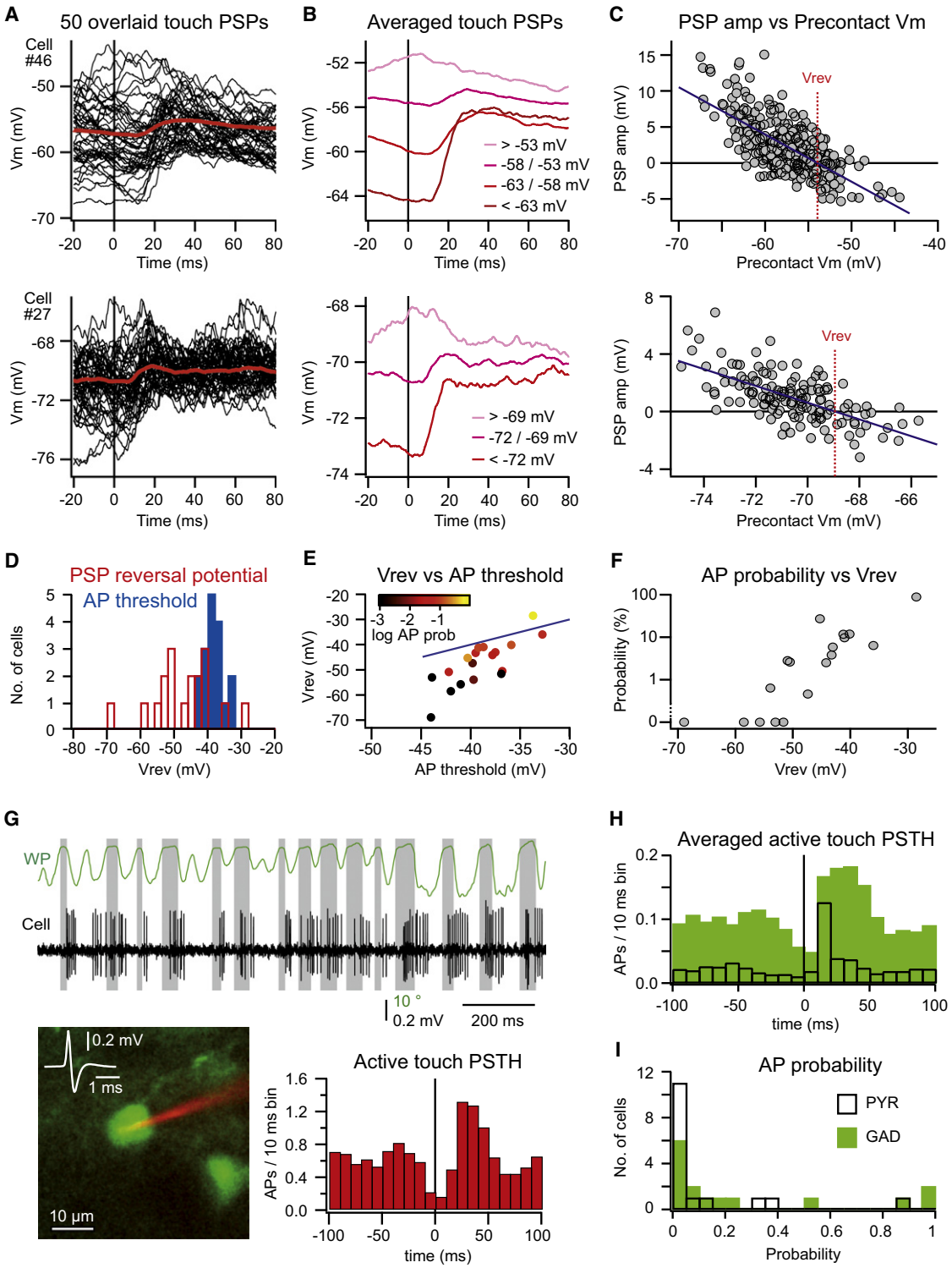

Figure 5. Hyperpolarized Reversal Potentials of Touch-Evoked PSPs Drive Sparse Coding

(A) Overlaid consecutive touch responses illustrate the high variability of the touch-evoked postsynaptic potentials. Two example recordings are shown (cell #46 above; cell #27 below).

(B) Averaged touch responses for different precontact Vm ranges. Note the hyperpolarizing touch-evoked PSPs from the most depolarized values of precontact Vm.

(C) The touch-evoked PSP amplitude is linearly correlated with precontact Vm, revealing hyperpolarized reversal potentials (Vrev).

response was quantified by an exponential fit, yielding the intercontact interval time-constant for the half-maximal response, which we denote as ICI_{50}. The time course of suppression of the touch response varied strongly across the population of recorded neurons with a mean ICI_{50} of 87 ± 61 ms (median 63 ms; range 14 to 194 ms). Across our population of recorded C2 column layer 2/3 neurons, the mean amplitude of the touch response for long preceding ICI (>500 ms) was 8.3 ± 4.1 mV and decreased significantly to 3.1 ± 2.2 mV for short ICI (10–40 ms) (Figure 6J). The major impact of ICI on response variability could be seen by the linear relationship between the coefficient of variation of the response and the ICI_{50} (r = 0.94) (Figure 6K).

Since the duration of the touch response was often longer than the ICI, consecutive touch responses also in many cases began from a more depolarized baseline Vm. Indeed, plotting the precontact Vm against the preceding ICI indicates a near parallel increase in precontact Vm and decrease in response amplitude at shorter ICI (Figures 6C and 6G). Out of the 13 neurons showing a significant modulation of response amplitude by ICI, 11 showed also a significant modulation of precontact Vm by ICI (Table S2). A change in precontact Vm (Figures 6D and 6H) therefore provides a mechanistic explanation for the most important effects of ICI upon the touch-evoked PSP amplitude.

The simplest mechanism to account for these observations is that the adaptation of the subthreshold PSP amplitude could be due to a change in the electrical driving force, without the need for a decrease in touch-evoked synaptic conductances. If so the Vm at the peak of the response would be relatively unaffected by ICI. In agreement with this hypothesis, we found that the absolute Vm at the peak of touch response was remarkably stable in many neurons across ICI ranges (Figures 6B, 6C, 6F, and 6G) and contact number within a touch sequence (Figure 6I). Across the population the absolute Vm at the peak of the active touch response was −50.3 ± 8.6 mV for long ICI (>500 ms) and −50.5 ± 7.9 mV for short ICI (10–40 ms) (Figure 6J). The peak Vm at both short and long intercontact intervals was close to the reversal potential for each neuron (Figure 6J). Presumably as a consequence of the stable touch-evoked peak Vm, action potential firing was not significantly suppressed across consecutive touches (Figure 6I). Also consistent with this hypothesis, neurons with shorter-duration responses showed less adaptation with more rapid ICI_{50} recovery time-constants (Figure 6K). Equally, neurons recorded deeper in layer 2/3, which have shorter-duration PSPs (Figure 4B) also show less adaptation (faster ICI_{50}) of the PSP amplitude (Figure 6L).

Thus, in layer 2/3 pyramidal neurons of the C2 barrel column, a major part of the touch-by-touch PSP amplitude variability can be explained by the time course of the touch-evoked PSP, which decreases the subthreshold response amplitude of subsequent touch PSPs by decreasing the electrical driving force for excitatory synaptic input while increasing the driving force for inhibitory synaptic input. Interestingly, these Vm dynamics lead to a stable touch-evoked peak Vm in most neurons. However, it should be noted that in a small number of recordings (4 out of 17 neurons; Table S2), the peak Vm during successive touch responses decreased at short intercontact intervals (e.g., see Figure S4).

Touch Responses at Different Object Locations

We tested the response to active touch at two different object positions in ten layer 2/3 neurons in the C2 barrel column (seven pyramidal and three unidentified cells) (Figure 7A). The objects were rapidly introduced by piezoactuators into the whisker path at two fixed locations at the same radial distance from the whisker pad (Movie S2). Whisker contacts with objects at different rostrocaudal locations evoked different touch responses (Figures 7A and 7B). This difference was significant in 5/10 neurons (Figure 7E), with the response to contact being bigger at the more rostral position in 4 out of 5 cells. In our experiments, whisker-object contacts always occurred near the most protracted phase of the whisking cycle, precluding analysis of phase relationship with touch response (Curtis and Kleinfeld, 2009). Mice made smaller and more frequent contacts during active touch of a near object (position 1, caudal). During active palpation of objects located further forward (position 2, rostral), mice made larger-amplitude whisker protraction movements at lower frequencies (Figure 7D). Retraction motor commands from sensory cortex might contribute to organizing these touch-evoked changes in whisker movement (Matyas et al., 2010).

The differences in whisking movements during active touch of objects at near and far positions appeared to account for the most important differences in touch responses evoked at these locations. We found that changes in ICI drove a substantial part of the observed differences in touch responses. Selecting for touch responses with similar ICI range at each of the two object locations revealed strikingly similar touch responses (Figure 7B). Furthermore, the distribution of response amplitudes as a function of the ICI for the two positions (Figure 7C) were not significantly different in most of the recordings (8/10) (Table S2). The experimentally measured difference in response

(D) The distribution of action potential threshold and Vrev for the touch PSP across the data set.
(E) Vrev plotted as a function of action potential threshold for each neuron in the data set. The line of unity is indicated in blue. The logarithmic scale color-coding of each data point indicates the probability of touch-evoked action potential firing for the given neuron.
(F) The probability of touch-evoked action potential firing (log scale) was strongly dependent upon Vrev ($p < 0.001$, Spearman's rank correlation test).
(G) Juxtacellular recording from a GFP-labeled GABAergic neuron (upper trace; green trace shows whisker position, black trace shows the extracellular potential and gray indicates whisker-object contact times) and the touch-evoked PSTH (lower right). The two photon image in the lower left shows the green GABAergic neuron contacted by the red Alexa594-filled recording electrode (inset shows the fast-spike waveform of this neuron).
(H) Grand-average PSTH for juxtacellular recordings from GFP-labeled GABAergic neurons (green filled bars, n = 15) and from juxtacellular recordings from excitatory neurons (black open bars, n = 16).
(I) Distribution of touch-evoked action potential probability measured in juxtacellular recordings. GABAergic neurons fired at significantly higher rates than excitatory neurons during active touch.

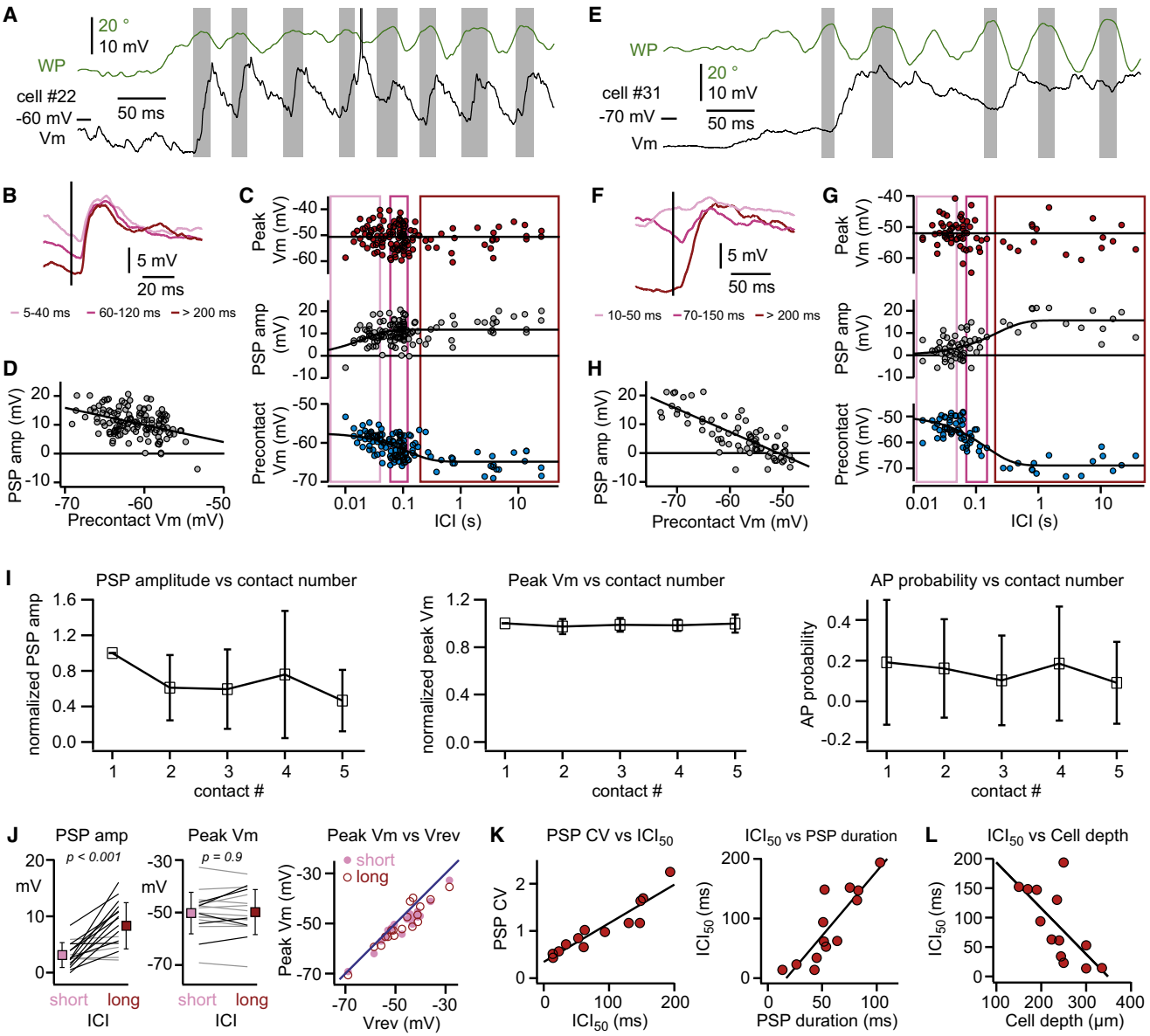

Figure 6. Intercontact Interval Is a Key Determinant of the Touch Response

(A–H) Two example recordings from different layer 2/3 pyramidal neurons within the C2 barrel column showing weak (A–D, cell #22) or strong (E–H, cell #31) modulation of the active touch subthreshold response by intercontact interval (ICI). Whisker position (WP, green), Vm (black, action potentials are truncated), and whisker-object contacts (gray bars) showing the response to successive active touches (A and E). Averaged responses for three different ICI ranges (B and F). Plots showing peak response Vm, PSP response amplitude, and precontact Vm as function of ICI on a log scale (C and G). Colored rectangles (C and G) indicate ICI ranges used for response averages (B and F). The amplitude of the response is linearly correlated to the precontact Vm (D and H).

(I) PSP amplitude (left), peak evoked Vm (middle), and action potential probability in the 50 ms following each contact (right) as a function of contact number quantified across all recordings. Data are shown as mean ± SD.

(J) Mean PSP response amplitude (left) and peak Vm depolarization of the touch response (middle) computed for short (10–40 ms) and long (>500 ms) ICI. Each line represents one neuron (gray, nonsignificant difference; black, significant difference), squares indicate population mean ± SD. Peak Vm as a function of the PSP reversal potential for each neuron at both short (pink circles) and long (red circles) ICI (right, blue line indicates line of unity).

(K) There is a linear relationship between PSP coefficient of variation (CV) versus ICI_{50} ($r = 0.94$) and also between ICI_{50} versus half-amplitude response duration ($r = 0.86$) (linear correlation with t statistics, $p < 0.001$).

(L) Neurons deeper in layer 2/3 have faster PSP recovery time constants (ICI_{50}) from preceding contacts ($r = -0.68$; $p < 0.05$).

amplitude for the two positions was reduced to less than 1 mV in 8/10 neurons when responses were evaluated at a matched ICI (Figure 7E). Equally, the touch-evoked PSP reversal potential was strikingly similar for the two object positions in most neurons (Figure 7E). Thus, under our experimental conditions, encoding of object location in layer 2/3 neurons of primary somatosensory

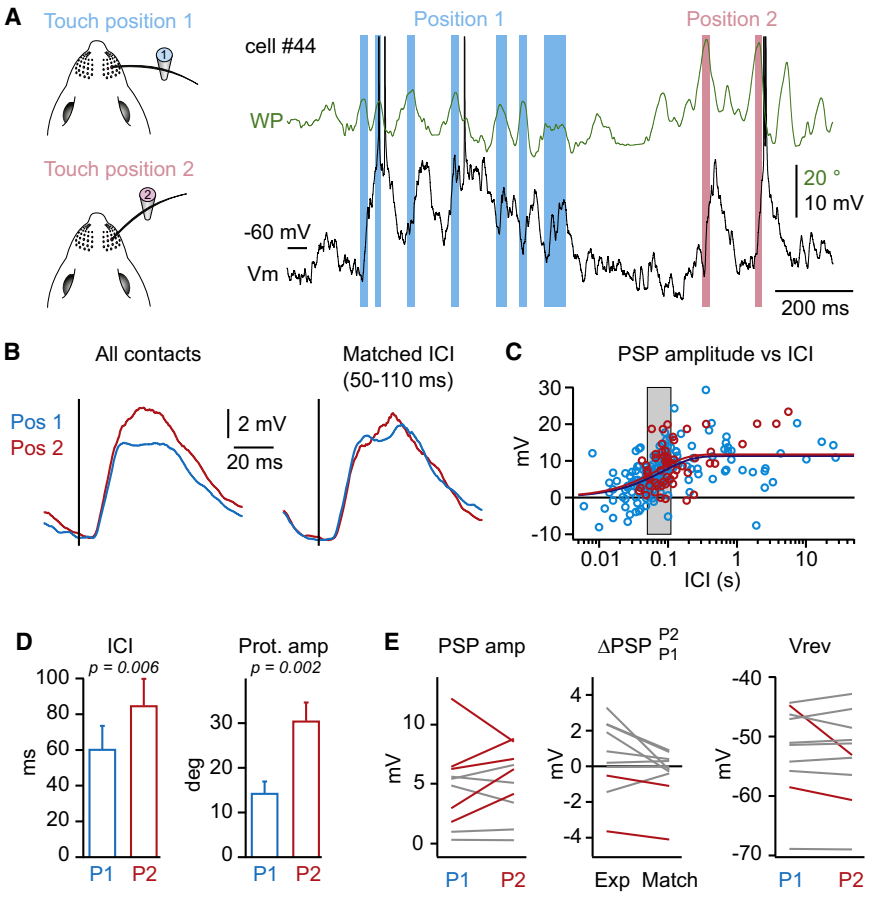

Figure 7. Object Location Encoding through Intercontact Interval

(A) Schematic drawing of the experimental paradigm and an example experiment showing the response of a layer 2/3 pyramidal neuron within the C2 barrel column (cell #44) to whisker-object contacts for caudal (position 1, blue) and rostral (position 2, red) object locations; whisker position (WP, green), membrane potential (Vm, black, action potentials are truncated), and whisker object contacts are shown (blue and red bars).

(B) For the same cell as shown in (A), averaged responses to active touch for the two object locations (position 1, caudal, blue; position 2, rostral, red) including all contacts (left) or after matching touch responses at the same intercontact interval (ICI) range (50–110 ms) (right).

(C) For the same cell as shown in (A) and (B), the distribution of PSP response amplitudes as a function of the ICI for object position 1 (caudal, blue) and position 2 (rostral, red) fitted separately with exponential recovery functions (blue and red lines); the gray rectangle indicates the range used for matching ICI (B, right).

(D) Across the population, the median ICI (left) is longer for touch of the rostral object at position 2 (P2, red) compared to the caudal object at position 1 (P1, blue). The mean whisker protraction amplitude (right) was larger before touch of the rostral object at position 2 (P2, red) compared to the caudal object at position 1 (P1, blue). Data are shown as mean ± SD.

(E) Mean PSP response amplitude for the two object positions including all contacts (left; each line corresponds to one neuron with gray for nonsignificant difference and red for significant difference). Difference in PSP response amplitude (PSP position 2 – PSP position 1) for experimentally measured responses with all contacts included (Exp) and for the computed difference for matched ICI obtained from the fitted exponential recovery curves (Match) (center; lines indicate individual neurons with significant (red) or nonsignificant (gray) differences in the distribution of PSP amplitude versus ICI for the two object positions). The reversal potential of the touch-evoked response was not different comparing the two object positions for most neurons (right, color coding as for center panel).

barrel cortex appears to result in large part from differences in motor control.

However, in two neurons the difference in ICI could not explain the difference in response amplitude between the two locations. One of these cells (cell #22, Figure S5) was also one of the few neurons showing strong and reliable modulation of Vm by whisker movements during free whisking (Figure S1), suggesting important interactions between fast Vm modulation during free whisking and the active touch signals in a small number of layer 2/3 excitatory neurons.

Highly Correlated Membrane Potential Dynamics during Active Touch

Given that touch responses varied across different neurons and that touch responses exhibit substantial touch-to-touch variability, we wondered whether the correlations of Vm dynamics of nearby neurons would increase or decrease during active touch. In order to directly measure Vm correlations, we analyzed dual whole-cell recording data from eight pairs of nearby neurons (Table S1) (Poulet and Petersen, 2008). Pairs of recorded neurons were within a few hundred microns of each other. Touch-evoked synchronous depolarizations were robustly observed in dual recordings during active touch (Figures 8A and 8B). Plotting the amplitude of the touch response recorded in one cell against the amplitude of the touch response in the other cell revealed a linear correlation (Figure 8C), which was significant in 7/8 neurons with mean correlation 0.46 ± 0.19 (median 0.48; range 0.13 to 0.69). Overall increases in Vm cross-correlations during touch sequences (Figure 8D) are likely to be driven through touch-by-touch correlations in response amplitude in pairs of neurons with similar touch response dynamics (Figure 8E). Whereas membrane potentials decorrelate during free-whisking periods compared to quiet wakefulness (Poulet and Petersen, 2008; Gentet et al., 2010), they again become more correlated during active touch. This recorrelation not only increases the peak cross-correlation value (quiet 0.65 ± 0.12; whisking 0.37 ± 0.16; touch 0.53 ± 0.12) (Figure 8F), but it also reduces the width of the correlation (quiet 95.1 ± 20.6 ms; whisking 59.9 ± 16.6 ms; touch 53.6 ± 15.4 ms) (Figure 8G). Vm synchrony therefore increases in magnitude and becomes temporally more precise during active touch. Interestingly, a negative correlation was found between Vm cross-correlation amplitude during active

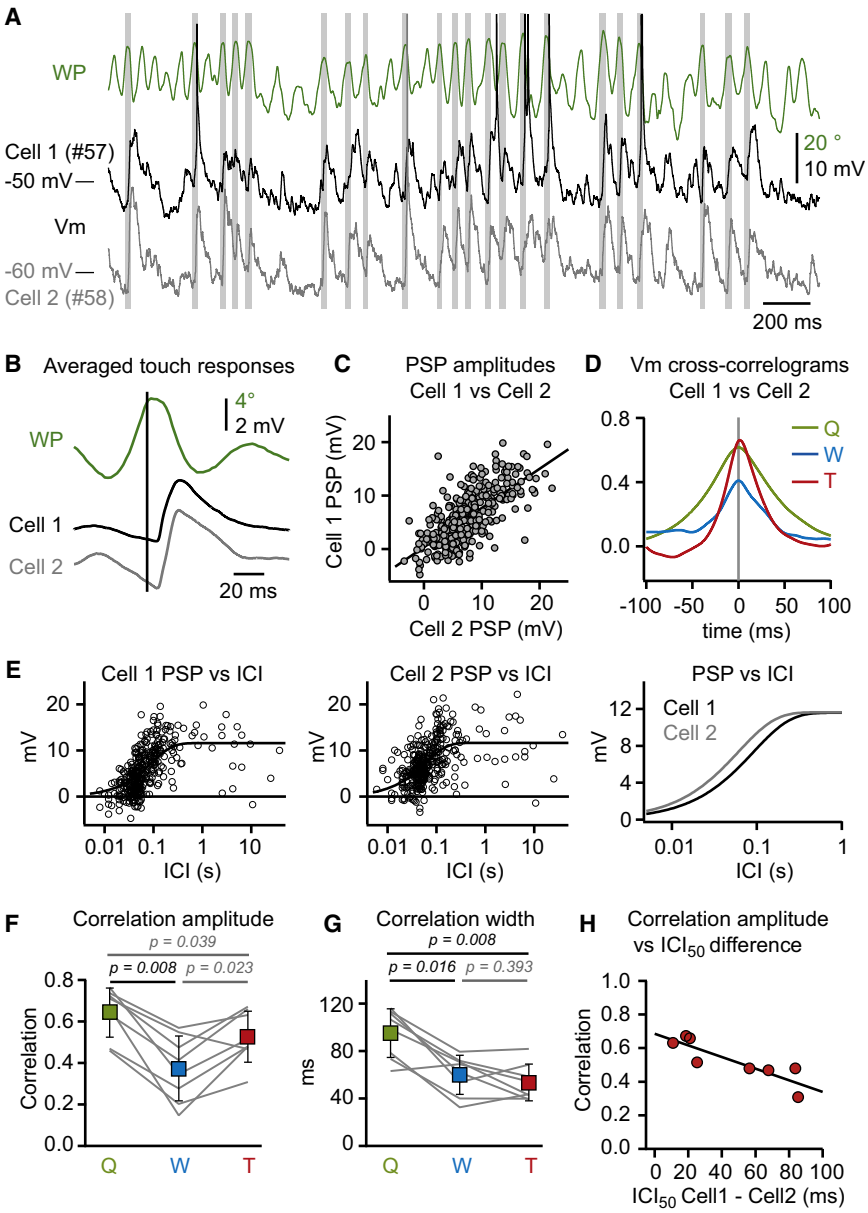

Figure 8. Membrane Potential during Active Touch is Highly Correlated in Nearby Layer 2/3 Neurons

(A) An example of a simultaneous dual whole-cell recording across a sequence of active whisker-object contacts; whisker position (WP, green), Vm cell 1 (black) and cell 2 (gray) (action potentials are truncated), and whisker-object contacts (gray bars) are shown.

(B) The whisker-object contact triggered averaged WP, Vm cell 1, and Vm cell 2 (same recording as A).

(C) The touch-by-touch PSP response amplitude covaried in cells 1 and 2 (same recording as A and B).

(D) Averaged cross-correlations between Vm of cell 1 and cell 2 for quiet (Q, green), free whisking (W, blue), and active touch (T, red) (same recording as A–C).

(E) Response amplitude as function of ICI for cells 1 and 2 and overlay of the two fitted exponential recovery functions (same recording as A–D).

(F and G) The amplitude (F) and width (G) of the Vm cross-correlation during quiet (Q, green), free whisking (W, blue) and active touch (T, red) across eight dual recordings (each line represents one paired recording; squares represent population mean ± SD). Significance was assessed using the Wilcoxon Signed Rank test; p values in black and gray indicate significant and nonsignificant differences, respectively, after Bonferonni correction ($p < 0.016$).

(H) The amplitude of cross-correlation during active touch was negatively correlated to the difference in ICI_{50} between two simultaneously recorded neurons ($r = -0.87$; linear correlation with t statistics; $p < 0.01$).

touch and the difference in ICI_{50} between cells (Figure 8H). Thus subthreshold membrane potential dynamics are more correlated in neurons sharing similar sensory response dynamics.

DISCUSSION

Recordings from animals actively sensing their environment are of critical importance for understanding perception. During natural animal behavior, most tactile sensory information is actively acquired through self-generated movements and sensory perception must therefore result from sensorimotor integration. Whereas previous measurements of mammalian active sensorimotor processing were made with extracellular recordings, here we applied the whole-cell recording technique, which offers insight into the synaptic computations taking place in individual neurons.

Sparse Coding and Reversal Potential

Although all layer 2/3 pyramidal neurons of the aligned cortical column depolarized in response to active touch, only a few fired action potentials with high probability to each whisker-object contact. The sparse action potential activity is not an artifact resulting from the whole-cell recording technique since juxtacellular recordings provided very similar results (Figure 4A). The overall low firing probability of layer 2/3 pyramidal cells observed in this study is in good agreement with recent juxtacellular recording studies from identified excitatory neurons in awake head-restrained rodents (de Kock and Sakmann, 2009; Sakata and Harris, 2009) but contrasts with the higher firing rates reported by extracellular recordings of unidentified neurons in freely moving animals (Krupa et al., 2004; von Heimendahl et al., 2007; Jadhav et al., 2009; Curtis and Kleinfeld, 2009; Vijayan et al., 2010). The higher firing rates in these studies could result from differences in the sample of neurons recorded: (1) extracellular recordings often target deeper layers, where firing

rates are higher (de Kock and Sakmann, 2009; Sakata & Harris, 2009); (2) extracellular recordings will include contributions from non-fast-spiking GABAergic neurons, which fire at higher rates and whose spike waveform cannot be distinguished from excitatory neurons (Liu et al., 2009; Gentet et al., 2010); and (3) the inherent bias in extracellular recordings which require neurons to fire action potentials before they can be considered in the data set (cells that do not fire or fire very rarely cannot be detected). Future experiments must directly investigate whether firing rates (and firing correlations) differ depending upon the behavioral conditions, for example running versus stationary (Niell and Stryker, 2010) and/or the complexity of the sensory input and the environment (multiple whiskers contacting textured objects compared to single whisker contacts with simple objects). Under our recording conditions we find a highly skewed distribution of spiking activity in layer 2/3 barrel cortex neurons during active touch, which leads to an interesting unresolved issue of sparse coding regarding the relative importance of the very few neurons that reliably fire many action potentials compared to the very many neurons that fire few action potentials.

We found that sparse action potential firing during active touch appeared to be enforced by the hyperpolarized reversal potential of the touch response. Indeed, we found close to linear relationships in individual neurons between PSP amplitude and precontact membrane potential with reversal potentials usually hyperpolarized with respect to action potential threshold. If the precontact membrane potential is spontaneously depolarized above this reversal potential, then the touch response is hyperpolarizing, therefore in fact playing an inhibitory role by preventing the membrane potential from reaching action potential threshold. Each neuron has its own cell-specific reversal potential for the touch response. Importantly, we found a strong positive correlation of the touch-evoked firing probability with the reversal potential (Figure 5F). Indeed, the only neuron in our study that fired reliably during active touch was also the only neuron with a touch reversal potential above action potential threshold.

The generally hyperpolarized reversal potentials suggest a prominent inhibitory GABAergic contribution to the active touch responses, since the reversal potential for glutamatergic excitatory postsynaptic potentials is close to 0 mV and the reversal potential for GABAergic inhibitory postsynaptic potentials is generally estimated between −70 and −90 mV. We find that GABAergic neurons are strongly recruited during active touch and they are therefore likely to contribute to driving the hyperpolarized reversal potential of the touch PSP, thus preventing the membrane potential from crossing action potential threshold for most neurons during active touch. Our results are consistent with the simple idea that active touch for a given cell evokes a well-defined mixture of excitatory and inhibitory conductances, which drive the membrane potential toward a specific reversal potential. However, our measurements do not rule out that there could be important contributions from changes in the overall network activity. The reversal potential that we define here is based on differences in the spontaneous precontact membrane potential and given that neuronal network activity is significantly correlated, there could be important differences in the underlying synaptic conductances driving the touch-evoked membrane potential response from different precontact membrane potentials.

Future studies should investigate the synaptic and intrinsic conductances driving membrane potential dynamics during active touch. Excitatory and inhibitory synaptic inputs are distributed across the complex dendritic arbors of the pyramidal neurons and the electrical signals are strongly filtered and attenuated as they propagate toward the soma (Nevian et al., 2007). In addition, there are several potential sources for nonlinear dendritic interactions including NMDA receptors as well as voltage-gated sodium, potassium, and calcium channels (Losonczy et al., 2008; Branco et al., 2010). Voltage-clamp measurements would offer the possibility for direct measurement of the underlying synaptic conductances, but this technique suffers from space-clamp errors, which might severely affect results (Williams and Mitchell, 2008). Carefully interpreted experiments are therefore necessary to quantitatively describe the synaptic conductance dynamics driving the physiologically relevant PSPs with hyperpolarized reversal potentials that we have studied here.

Active Touch Response Variability and Dynamics

A prominent feature of the touch response in individual neurons was the high touch-by-touch variability (Figure 5). The precontact membrane potential accounted for a large part of the PSP variance and mechanistically explained the dynamics of touch responses evoked at different intercontact intervals (Figure 6), as well as forming a basis for a motor encoding of object position (Figure 7). Touch-evoked PSPs were strongly reduced at short intercontact intervals, probably due to long-lasting PSPs depolarizing the precontact membrane potential for subsequent touch responses. However, in most cells, the absolute membrane potential reached during the peak of the touch response was unaffected by intercontact interval. Each touch therefore appears to drive the membrane potential toward a cell-specific reversal potential, which in most neurons is a well-defined value independent of intercontact interval (Figure 6J) or object location (Figure 7E). The overall effect of a C2 whisker touch on the excitatory layer 2/3 neurons of the C2 barrel column is perhaps best described as a transient activation of synaptic conductances pushing the neuronal network toward a state vector of cell-specific reversal potentials.

These dynamics of active touch responses in awake exploring mice differ markedly from results obtained under anesthesia, which show strong depression of peak membrane potential depolarization and action potential firing in layer 2/3 during repetitive passive whisker-deflection (Ahissar et al., 2000; Brecht et al., 2003; Higley and Contreras, 2006; Heiss et al., 2008). The decreased sensory response during repetitive passive whisker stimulation under anesthesia has been ascribed to a decrease in synaptic inputs (Higley and Contreras, 2006; Heiss et al., 2008), which could partly result from short-term depression of thalamocortical synapses (Chung et al., 2002; Castro-Alamancos, 2004; Katz et al., 2006). In awake animals, in contrast, sensory responses evoked by electrical stimulation of the infraorbital nerve show little adaptation (Castro-Alamancos, 2004), in agreement with our data from awake mice actively

sensing natural stimuli. Differences in sensory adaptation comparing awake and anesthetized animals might result from differences in the functional operation of cortical circuits during different brain states (Crochet and Petersen, 2006; Poulet and Petersen, 2008; Gentet et al., 2010). Differences in thalamic activity are also likely to play an important role. Short-term depression of thalamocortical synapses is prominent under anesthesia (Ahissar et al., 2000; Chung et al., 2002; Khatri et al., 2004; Katz et al., 2006), but firing rates in the thalamus are increased during active waking, perhaps maintaining thalamocortical synapses at a level of steady-state depression (Fanselow and Nicolelis, 1999; Castro-Alamancos, 2004).

Importantly, it should be noted that we could only account for a part of the touch-by-touch variability of active touch responses. Associational, attentional, motor and other top-down inputs are also likely to contribute to the membrane potential fluctuations of layer 2/3 pyramidal neurons during active touch. Equally touch-by-touch variation in the excitatory and inhibitory conductances evoked by whisker-object contact is likely to contribute to determining which touch responses drive the low probability action potential firing observed in most layer 2/3 pyramidal neurons.

Functional Organization within Layer 2/3

The amplitude, kinetics, and dynamics of the active touch response varied across the neuronal population (Figures 3 and 4). Our study revealed a functional organization among layer 2/3 pyramidal neurons. Deeper pyramidal neurons in layer 3 on average responded with larger amplitude, shorter latency, and shorter-duration touch responses and showed only moderate adaptation of the PSP amplitude compared to more superficial pyramidal neurons in layer 2. Glutamatergic excitatory synaptic inputs from layers 3 and 4, as well as from the VPM thalamus, onto layer 3 neurons probably contribute to driving these large and rapid responses, which robustly signal the timing of each individual whisker-object contact. Consistent with a peripheral sensory origin of the fast phase-locked membrane potentials during free whisking (Poulet and Petersen, 2008), layer 3 neurons also had stronger free whisking Vm modulation compared to layer 2 neurons (Figure S1).

Superficial pyramidal neurons located in layer 2 on average responded with smaller amplitude touch responses with longer latency and longer duration. The layer 2 pyramidal neurons are likely to be driven primarily by intracortical synaptic circuits, receiving prominent excitatory inputs from layers 2, 3, 4, and 5A (Bureau et al., 2006; Lübke and Feldmeyer, 2007; Schubert et al., 2007; Lefort et al., 2009). Through these intracortical inputs, the layer 2 neurons therefore may serve as integrators of sensory tactile information across multiple contacts.

Highly Correlated Membrane Potential Dynamics during Active Touch

Dual whole-cell recordings provided insight into the membrane potential correlations of nearby layer 2/3 neurons during behavior. During quiet waking, in the absence of whisker movement, barrel cortex neurons exhibit slow large-amplitude membrane potential oscillations (Figures 1 and 2), which are synchronous in nearby neurons (Poulet and Petersen, 2008; Gentet et al., 2010) and occur as propagating waves of activity across large cortical regions (Ferezou et al., 2007). During active exploratory periods of free whisking, layer 2/3 pyramidal neurons depolarize and the slow large-amplitude membrane potential oscillations are suppressed (Figures 1 and 2), through an internally generated change in brain state (Poulet and Petersen, 2008). Membrane potentials are less correlated in nearby neurons during free whisking (Figure 8) and membrane potential variance is low (Figure 2), with small-amplitude membrane potential oscillations locked to whisker movement at cell-specific phases (Figure S1). As the whisking mouse encounters an object, each C2 whisker touch evokes a depolarizing sensory response in every layer 2/3 pyramidal neuron of the C2 barrel column (Figures 3 and 4). However, unlike the experimenter, the mouse does not a priori know when the whisker contacts an object. Detection of the whisker-object contact for the mouse is probably enhanced by the relatively low variance and decorrelated spontaneous membrane potential fluctuations during free whisking, which contrast with the highly correlated and temporally precise membrane potential dynamics during active touch driven by rapid and large amplitude touch-evoked depolarizations (Figure 8). The membrane potentials in neurons with similar sensory response dynamics were particularly highly correlated during active touch, pointing to a specific synchronization of functional subnetworks within a cortical column reminiscent of the Hebbian concept of "cell assemblies."

Future Perspectives

Sparse action potential firing within a synchronized neuronal network therefore encodes the active touch of whisker and object in layer 2/3 pyramidal neurons of mouse barrel cortex. The sparse coding appears to result from the hyperpolarized reversal potential of the touch-evoked PSPs, which prevents the cell from reaching spike threshold. Only cells with depolarized reversal potentials could fire action potentials reliably in response to active touch. Our membrane potential measurements in behaving mice begin to provide synaptic and mechanistic explanations for the sparse action potential coding in supragranular cortical layers (de Kock and Sakmann, 2009; Sakata and Harris, 2009; O'Connor et al., 2010) and point to a critical role for inhibitory GABAergic neurons in gating active touch sensory responses in supragranular pyramidal cells (Gabernet et al., 2005; Sun et al., 2006; Haider et al., 2010; Cruikshank et al., 2010). Future studies should define more precisely the role of different subtypes of inhibitory GABAergic neurons during active touch, which can now be approached through two photon targeted recordings of cell-type-specific GFP-expressing mouse lines (Margrie et al., 2003; Liu et al., 2009; Gentet et al., 2010) or by selectively manipulating cortical neuron subpopulations during functional operation through combinations of optogenetics, viral gene transduction, and mouse genetics (Boyden et al., 2005; Cardin et al., 2009; Sohal et al., 2009). Through such further experimentation in combination with computational modeling, it will be of great interest to investigate the circuit determinants of the hyperpolarized touch-evoked reversal potentials and whether the PSP reversal potential is fixed for a given neuron or whether it can be modulated by context, behavior, and learning.

Here, in this study, we provide detailed measurements of the synaptically driven membrane potential dynamics of identified neurons within a specific well-defined cortical column in actively sensing mice. Such data form an essential step toward a causal and mechanistic explanation for the functional operation of neocortical microcircuits during behavior at the level of individual neurons and their synaptic inputs.

EXPERIMENTAL PROCEDURES

The experimental procedures are described in detail in the Supplemental Information.

Animal Preparation

All experimental procedures were approved by the Swiss Federal Veterinary Office. C57BL6J or GAD67-GFP mice were implanted with a metal head-fixation post and trained for head-restraint. All whiskers of the mouse except C2 were trimmed before the recording session. The left C2 barrel column was functionally located using intrinsic optical imaging (Grinvald et al., 1986) through the intact bone (Ferezou et al., 2006). A small craniotomy (<0.5 mm in diameter) was then opened to allow for the insertion of the patch pipette within the C2 barrel column. The recording chamber was filled with Kwik-Cast (WPI) to protect the exposed brain and the animal recovered in its cage for 2-4 hr before the recording session began.

Electrophysiology and Quantification of Whisker Behavior

Electrophysiological recordings, targeted to the C2 barrel column identified by intrinsic optical imaging, were carried out following previously described methods (Crochet and Petersen, 2006; Poulet and Petersen, 2008; Gentet et al., 2010). The whole-cell recording solution contained (in mM): 135 potassium gluconate, 4 KCl, 10 HEPES, 10 sodium phosphocreatine, 4 MgATP, 0.3 Na_3GTP (adjusted to pH 7.3 with KOH), and 2 mg/ml biocytin (for post-hoc anatomical identification). The Vm was not corrected for liquid junction potential.

Juxtacellular recordings in GAD67-GFP mice (Tamamaki et al., 2003) were targeted through two-photon microscopy to neuronal somata under visual control. The juxtacellular configuration was attested by a high electrical resistance and positive spike waveforms. Recordings were included in the database only if at least one AP could be detected both before and after the recording.

Short (20–30 s) sweeps were recorded while the whisker behavior of the mouse was simultaneously filmed using a high-speed camera (MotionPro, Redlake) operating at 500 frames per second. The behavioral images were synchronized to the electrophysiological recording through TTL pulses. Whisker movements and whisker-object contacts were quantified off-line.

Object Presentation and Contact Detection

Two protocols were used to examine active touch of the C2 whisker with an object. In one set of experiments, a metal bar was moved close to the animal so that the mouse could actively palpate the object by whisking. In a second set of experiments we used a custom-built piezo-based system allowing a rapid introduction of an object into the path of the whisker at two locations. All experiments relating to object position coding were carried out using the piezoactuator protocol allowing rapid introduction and removal of objects on the millisecond timescale. Contact onset was defined by the first change in whisker curvature as the whisker advanced against the object.

Histology and Cell Identification

Tangential slices 100 μm thick containing the layer 4 barrel field were stained for cytochrome oxidase to reveal the barrel map and subsequently all slices were stained for biocytin (ABC-Elite; Vector Laboratories). Cell type identification was based on dendritic arborization and presence of dendritic spines. Cell location within the barrel map was determined by tracking the axon down to layer 4, where barrels could be visualized by the cytochrome oxidase staining. Neuronal reconstruction was performed using Neurolucida (MicroBrightField).

Data Analysis

Data analysis was performed using IgorPro (see Supplemental Experimental Procedures). All values are mean ± SD. Nonparametric statistical tests were used to assess significance (Wilcoxon-Mann-Whitney two-sample rank test or Wilcoxon Signed Rank test) and the relationship between two variables (Spearman's rank correlation test). When appropriate, linear correlation with *t* statistics was used.

SUPPLEMENTAL INFORMATION

Supplemental Information includes Supplemental Experimental Procedures, two tables, five figures, and two movies and can be found with this article online at doi:10.1016/j.neuron.2011.02.022.

ACKNOWLEDGMENTS

This work was funded by grants from the Swiss National Science Foundation (CCHP), Human Frontiers in Science Program (J.F.A.P. and C.C.H.P.), SystemsX.ch (C.C.H.P.), Deutsche Forschungs Gemeinschaft (J.F.A.P.), and Agence Nationale de la Recherche, France (S.C.).

Accepted: January 11, 2011
Published: March 23, 2011

REFERENCES

Ahissar, E., Sosnik, R., and Haidarliu, S. (2000). Transformation from temporal to rate coding in a somatosensory thalamocortical pathway. Nature *406*, 302–306.

Boyden, E.S., Zhang, F., Bamberg, E., Nagel, G., and Deisseroth, K. (2005). Millisecond-timescale, genetically targeted optical control of neural activity. Nat. Neurosci. *8*, 1263–1268.

Branco, T., Clark, B.A., and Häusser, M. (2010). Dendritic discrimination of temporal input sequences in cortical neurons. Science *329*, 1671–1675.

Brecht, M. (2007). Barrel cortex and whisker-mediated behaviors. Curr. Opin. Neurobiol. *17*, 408–416.

Brecht, M., Roth, A., and Sakmann, B. (2003). Dynamic receptive fields of reconstructed pyramidal cells in layers 3 and 2 of rat somatosensory barrel cortex. J. Physiol. *553*, 243–265.

Bruno, R.M., and Sakmann, B. (2006). Cortex is driven by weak but synchronously active thalamocortical synapses. Science *312*, 1622–1627.

Bureau, I., von Saint Paul, F., and Svoboda, K. (2006). Interdigitated paralemniscal and lemniscal pathways in the mouse barrel cortex. PLoS Biol. *4*, e382.

Buzsáki, G., and Draguhn, A. (2004). Neuronal oscillations in cortical networks. Science *304*, 1926–1929.

Cardin, J.A., Carlén, M., Meletis, K., Knoblich, U., Zhang, F., Deisseroth, K., Tsai, L.H., and Moore, C.I. (2009). Driving fast-spiking cells induces gamma rhythm and controls sensory responses. Nature *459*, 663–667.

Carvell, G.E., and Simons, D.J. (1990). Biometric analyses of vibrissal tactile discrimination in the rat. J. Neurosci. *10*, 2638–2648.

Castro-Alamancos, M.A. (2004). Absence of rapid sensory adaptation in neocortex during information processing states. Neuron *41*, 455–464.

Chung, S., Li, X., and Nelson, S.B. (2002). Short-term depression at thalamocortical synapses contributes to rapid adaptation of cortical sensory responses in vivo. Neuron *34*, 437–446.

Crochet, S., and Petersen, C.C.H. (2006). Correlating whisker behavior with membrane potential in barrel cortex of awake mice. Nat. Neurosci. *9*, 608–610.

Crochet, S., Chauvette, S., Boucetta, S., and Timofeev, I. (2005). Modulation of synaptic transmission in neocortex by network activities. Eur. J. Neurosci. *21*, 1030–1044.

Cruikshank, S.J., Urabe, H., Nurmikko, A.V., and Connors, B.W. (2010). Pathway-specific feedforward circuits between thalamus and neocortex revealed by selective optical stimulation of axons. Neuron *65*, 230–245.

Curtis, J.C., and Kleinfeld, D. (2009). Phase-to-rate transformations encode touch in cortical neurons of a scanning sensorimotor system. Nat. Neurosci. *12*, 492–501.

de Kock, C.P., and Sakmann, B. (2009). Spiking in primary somatosensory cortex during natural whisking in awake head-restrained rats is cell-type specific. Proc. Natl. Acad. Sci. USA *106*, 16446–16450.

Diamond, M.E., von Heimendahl, M., Knutsen, P.M., Kleinfeld, D., and Ahissar, E. (2008). 'Where' and 'what' in the whisker sensorimotor system. Nat. Rev. Neurosci. *9*, 601–612.

Fanselow, E.E., and Nicolelis, M.A.L. (1999). Behavioral modulation of tactile responses in the rat somatosensory system. J. Neurosci. *19*, 7603–7616.

Fee, M.S., Mitra, P.P., and Kleinfeld, D. (1997). Central versus peripheral determinants of patterned spike activity in rat vibrissa cortex during whisking. J. Neurophysiol. *78*, 1144–1149.

Ferezou, I., Bolea, S., and Petersen, C.C.H. (2006). Visualizing the cortical representation of whisker touch: voltage-sensitive dye imaging in freely moving mice. Neuron *50*, 617–629.

Ferezou, I., Haiss, F., Gentet, L.J., Aronoff, R., Weber, B., and Petersen, C.C.H. (2007). Spatiotemporal dynamics of cortical sensorimotor integration in behaving mice. Neuron *56*, 907–923.

Gabernet, L., Jadhav, S.P., Feldman, D.E., Carandini, M., and Scanziani, M. (2005). Somatosensory integration controlled by dynamic thalamocortical feed-forward inhibition. Neuron *48*, 315–327.

Gentet, L.J., Avermann, M., Matyas, F., Staiger, J.F., and Petersen, C.C.H. (2010). Membrane potential dynamics of GABAergic neurons in the barrel cortex of behaving mice. Neuron *65*, 422–435.

Gerdjikov, T.V., Bergner, C.G., Stüttgen, M.C., Waiblinger, C., and Schwarz, C. (2010). Discrimination of vibrotactile stimuli in the rat whisker system: Behavior and neurometrics. Neuron *65*, 530–540.

Greenberg, D.S., Houweling, A.R., and Kerr, J.N. (2008). Population imaging of ongoing neuronal activity in the visual cortex of awake rats. Nat. Neurosci. *11*, 749–751.

Grinvald, A., Lieke, E., Frostig, R.D., Gilbert, C.D., and Wiesel, T.N. (1986). Functional architecture of cortex revealed by optical imaging of intrinsic signals. Nature *324*, 361–364.

Guić-Robles, E., Valdivieso, C., and Guajardo, G. (1989). Rats can learn a roughness discrimination using only their vibrissal system. Behav. Brain Res. *31*, 285–289.

Haider, B., Krause, M.R., Duque, A., Yu, Y., Touryan, J., Mazer, J.A., and McCormick, D.A. (2010). Synaptic and network mechanisms of sparse and reliable visual cortical activity during nonclassical receptive field stimulation. Neuron *65*, 107–121.

Harris, J.A., Petersen, R.S., and Diamond, M.E. (1999). Distribution of tactile learning and its neural basis. Proc. Natl. Acad. Sci. USA *96*, 7587–7591.

Heiss, J.E., Katz, Y., Ganmor, E., and Lampl, I. (2008). Shift in the balance between excitation and inhibition during sensory adaptation of S1 neurons. J. Neurosci. *28*, 13320–13330.

Hentschke, H., Haiss, F., and Schwarz, C. (2006). Central signals rapidly switch tactile processing in rat barrel cortex during whisker movements. Cereb. Cortex *16*, 1142–1156.

Higley, M.J., and Contreras, D. (2006). Balanced excitation and inhibition determine spike timing during frequency adaptation. J. Neurosci. *26*, 448–457.

Hutson, K.A., and Masterton, R.B. (1986). The sensory contribution of a single vibrissa's cortical barrel. J. Neurophysiol. *56*, 1196–1223.

Jadhav, S.P., Wolfe, J., and Feldman, D.E. (2009). Sparse temporal coding of elementary tactile features during active whisker sensation. Nat. Neurosci. *12*, 792–800.

Katz, Y., Heiss, J.E., and Lampl, I. (2006). Cross-whisker adaptation of neurons in the rat barrel cortex. J. Neurosci. *26*, 13363–13372.

Khatri, V., Hartings, J.A., and Simons, D.J. (2004). Adaptation in thalamic barreloid and cortical barrel neurons to periodic whisker deflections varying in frequency and velocity. J. Neurophysiol. *92*, 3244–3254.

Knott, G.W., Quairiaux, C., Genoud, C., and Welker, E. (2002). Formation of dendritic spines with GABAergic synapses induced by whisker stimulation in adult mice. Neuron *34*, 265–273.

Knutsen, P.M., Pietr, M., and Ahissar, E. (2006). Haptic object localization in the vibrissal system: Behavior and performance. J. Neurosci. *26*, 8451–8464.

Krupa, D.J., Wiest, M.C., Shuler, M.G., Laubach, M., and Nicolelis, M.A. (2004). Layer-specific somatosensory cortical activation during active tactile discrimination. Science *304*, 1989–1992.

Lefort, S., Tomm, C., Floyd Sarria, J.C., and Petersen, C.C.H. (2009). The excitatory neuronal network of the C2 barrel column in mouse primary somatosensory cortex. Neuron *61*, 301–316.

Liu, B.-H., Li, P., Li, Y.-T., Sun, Y.J., Yanagawa, Y., Obata, K., Zhang, L.I., and Tao, H.W. (2009). Visual receptive field structure of cortical inhibitory neurons revealed by two-photon imaging guided recording. J. Neurosci. *29*, 10520–10532.

Losonczy, A., Makara, J.K., and Magee, J.C. (2008). Compartmentalized dendritic plasticity and input feature storage in neurons. Nature *452*, 436–441.

Lübke, J., and Feldmeyer, D. (2007). Excitatory signal flow and connectivity in a cortical column: Focus on barrel cortex. Brain Struct. Funct. *212*, 3–17.

Margrie, T.W., Meyer, A.H., Caputi, A., Monyer, H., Hasan, M.T., Schaefer, A.T., Denk, W., and Brecht, M. (2003). Targeted whole-cell recordings in the mammalian brain in vivo. Neuron *39*, 911–918.

Matyas, F., Sreenivasan, V., Marbach, F., Wacongne, C., Barsy, B., Mateo, C., Aronoff, R., and Petersen, C.C.H. (2010). Motor control by sensory cortex. Science *330*, 1240–1243.

Moore, C.I., and Nelson, S.B. (1998). Spatio-temporal subthreshold receptive fields in the vibrissa representation of rat primary somatosensory cortex. J. Neurophysiol. *80*, 2882–2892.

Nevian, T., Larkum, M.E., Polsky, A., and Schiller, J. (2007). Properties of basal dendrites of layer 5 pyramidal neurons: A direct patch-clamp recording study. Nat. Neurosci. *10*, 206–214.

Niell, C.M., and Stryker, M.P. (2010). Modulation of visual responses by behavioral state in mouse visual cortex. Neuron *65*, 472–479.

O'Connor, D.H., Peron, S.P., Huber, D., and Svoboda, K. (2010). Neural activity in barrel cortex underlying vibrissa-based object localization in mice. Neuron *67*, 1048–1061.

Okun, M., and Lampl, I. (2008). Instantaneous correlation of excitation and inhibition during ongoing and sensory-evoked activities. Nat. Neurosci. *11*, 535–537.

Petersen, C.C.H. (2007). The functional organization of the barrel cortex. Neuron *56*, 339–355.

Petersen, C.C.H., Hahn, T.T.G., Mehta, M., Grinvald, A., and Sakmann, B. (2003). Interaction of sensory responses with spontaneous depolarization in layer 2/3 barrel cortex. Proc. Natl. Acad. Sci. USA *100*, 13638–13643.

Poulet, J.F.A., and Petersen, C.C.H. (2008). Internal brain state regulates membrane potential synchrony in barrel cortex of behaving mice. Nature *454*, 881–885.

Sakata, S., and Harris, K.D. (2009). Laminar structure of spontaneous and sensory-evoked population activity in auditory cortex. Neuron *64*, 404–418.

Schubert, D., Kötter, R., and Staiger, J.F. (2007). Mapping functional connectivity in barrel-related columns reveals layer- and cell type-specific microcircuits. Brain Struct. Funct. *212*, 107–119.

Sohal, V.S., Zhang, F., Yizhar, O., and Deisseroth, K. (2009). Parvalbumin neurons and gamma rhythms enhance cortical circuit performance. Nature *459*, 698–702.

Stüttgen, M.C., and Schwarz, C. (2008). Psychophysical and neurometric detection performance under stimulus uncertainty. Nat. Neurosci. *11*, 1091–1099.

Sun, Q.Q., Huguenard, J.R., and Prince, D.A. (2006). Barrel cortex microcircuits: Thalamocortical feedforward inhibition in spiny stellate cells is mediated by a small number of fast-spiking interneurons. J. Neurosci. *26*, 1219–1230.

Tamamaki, N., Yanagawa, Y., Tomioka, R., Miyazaki, J., Obata, K., and Kaneko, T. (2003). Green fluorescent protein expression and colocalization with calretinin, parvalbumin, and somatostatin in the GAD67-GFP knock-in mouse. J. Comp. Neurol. *467*, 60–79.

Vijayan, S., Hale, G.J., Moore, C.I., Brown, E.N., and Wilson, M.A. (2010). Activity in the barrel cortex during active behavior and sleep. J. Neurophysiol. *103*, 2074–2084.

von Heimendahl, M., Itskov, P.M., Arabzadeh, E., and Diamond, M.E. (2007). Neuronal activity in rat barrel cortex underlying texture discrimination. PLoS Biol. *5*, e305.

Wilent, W.B., and Contreras, D. (2005). Dynamics of excitation and inhibition underlying stimulus selectivity in rat somatosensory cortex. Nat. Neurosci. *8*, 1364–1370.

Williams, S.R., and Mitchell, S.J. (2008). Direct measurement of somatic voltage clamp errors in central neurons. Nat. Neurosci. *11*, 790–798.

Zhu, J.J., and Connors, B.W. (1999). Intrinsic firing patterns and whisker-evoked synaptic responses of neurons in the rat barrel cortex. J. Neurophysiol. *81*, 1171–1183.